Grenfell et al., http://www.jcb.org/cgi/content/full/jcb.201604029/DC1

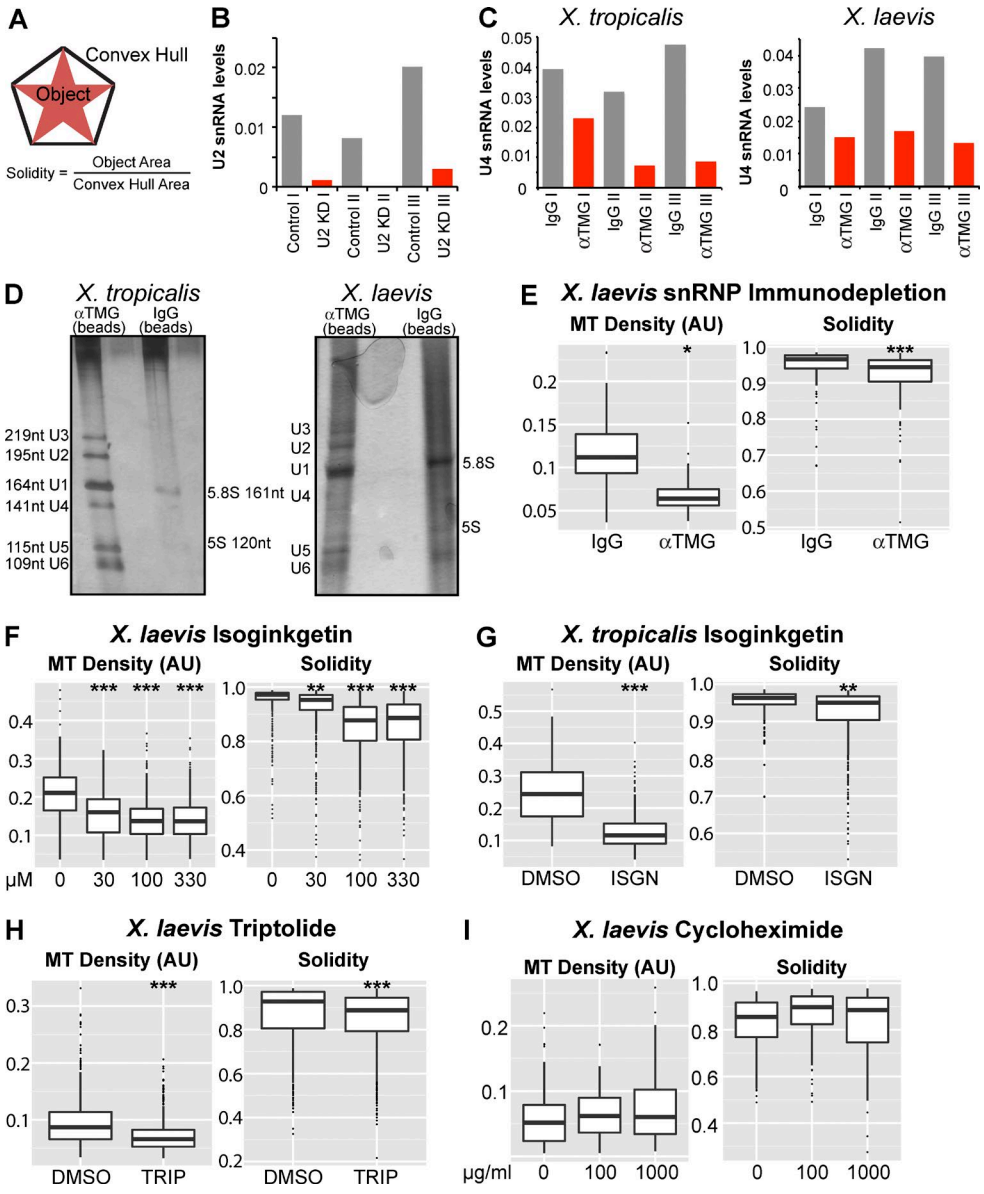

Figure S1. **Multiple RNA biogenesis perturbation strategies in *X. laevis* and *X. tropicalis* support a role for RNA processing in spindle assembly.** (A) Schematic explaining the solidity measurement used to quantify spindle morphology defects. Solidity is defined as the area of the object (spindle) divided by the area of the convex hull. (B) qPCR quantification of U2 snRNA knockdown efficiency in *X. laevis* compared with a histone H3 reference transcript. Three independent experiments are shown (I–III). (C) qPCR quantification of splicing factor immunodepletion efficiency. U4 snRNA was compared with 18S rRNA for *X. tropicalis* and 5S rRNA for *X. laevis*. TMG, snRNP immunodepletion with antibody K121 specific to the trimethylguanosine cap of core spliceosomal RNAs; IgG, nonspecific IgG (mock) depletion. Three independent experiments are shown (I–III). (D) Silver-stained PAGE gels showing RNAs enriched on TMG beads and IgG beads that were used in immunodepletion experiments. (E) Quantification of spindle microtubule density and solidity for *X. laevis* spindles formed after splicing factor immunodepletion (TMG, $n = 81$) compared with mock depletion (IgG, $n = 105$). Median microtubule density decreased 42.7% in splicing factor–depleted extract. (F) Quantification of spindle microtubule density and solidity for *X. laevis* spindles formed after ISGN treatment for an entire cell cycle (30 μM, $n = 359$; 100 μM, $n = 1{,}044$; 330 μM, $n = 965$) compared with DMSO ($n = 306$). Median microtubule density decreased 24.0% in 30 μM ISGN-treated extract, 35.1% in 100 μM ISGN-treated extract, and 35.2% in 330 μM ISGN-treated extract. (G) Quantification of spindle microtubule density and solidity for *X. tropicalis* spindles formed after ISGN treatment for an entire cell cycle ($n = 479$) compared with DMSO ($n = 407$). Median microtubule density decreased 52.5% in ISGN-treated extract. (H) Quantification of spindle microtubule density and solidity for *X. laevis* spindles formed after triptolide treatment for an entire cell cycle ($n = 996$) compared with DMSO ($n = 773$). Median microtubule density decreased 24.1% in triptolide-treated extract. (I) Quantification of spindle microtubule density and solidity after addition of the translation inhibitor cycloheximide at 100 μg/ml ($n = 100$) or 1,000 μg/ml ($n = 148$) compared with solvent controls ($n = 141$). Box plot horizontal lines correspond to the median value. Bottom and top of the boxes are first and third quartiles, respectively; whiskers show highest and lowest values within 1.5 times the interquartile range and outliers are plotted as single points. *, $P < 10^{-5}$; **, $P < 10^{-10}$; ***, $P < 10^{-15}$ (Kolmogorov–Smirnov test). AU, arbitrary units; MT, microtubule.

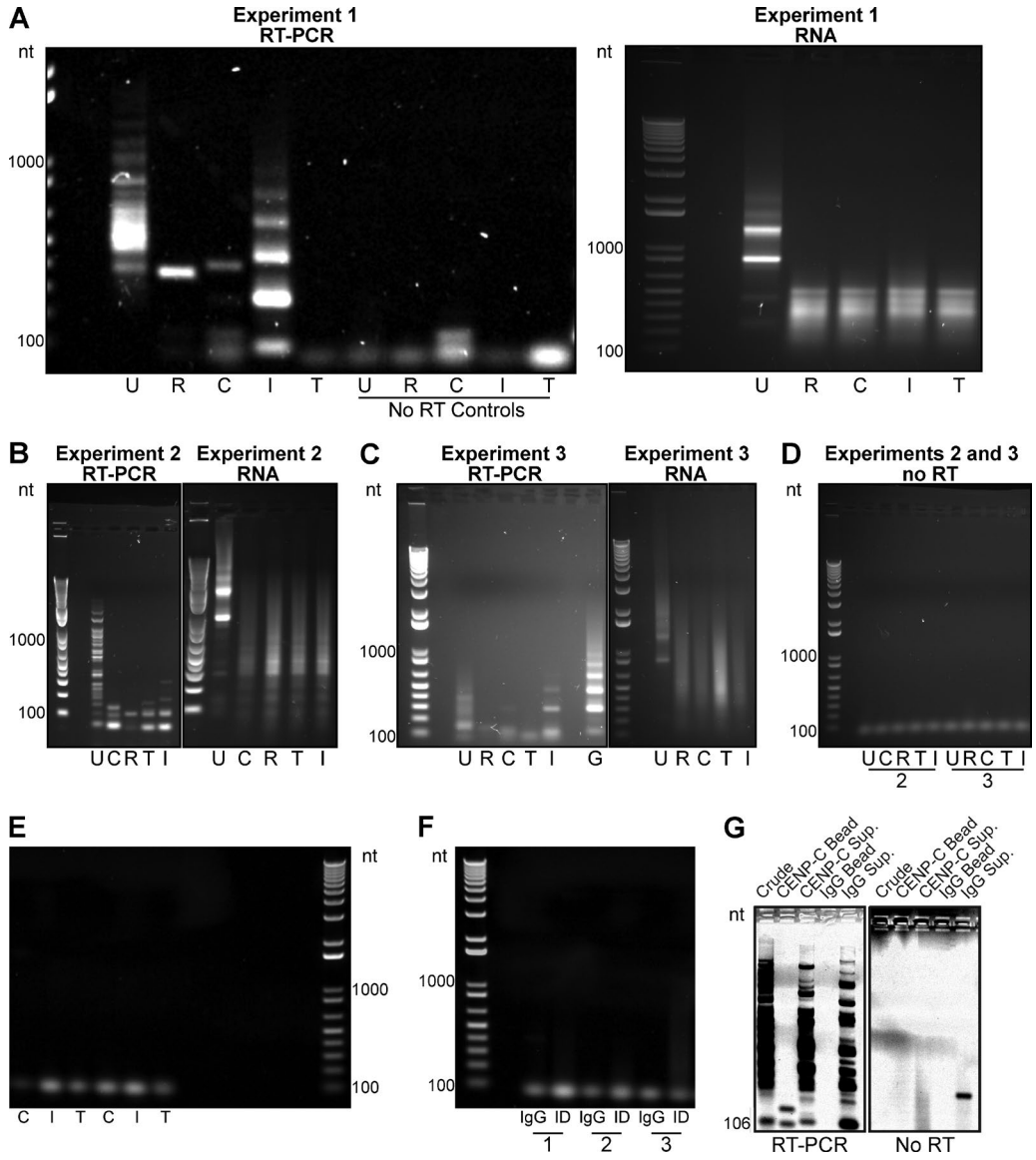

Figure S2. **The splicing machinery is involved in mitotic RNA biogenesis at the centromere.** Experimental replicates of the centromere RNA biogenesis assay in *X. laevis* extract. Letters indicate source of RNA used for PCR: U, untreated extract; R, RNase A–treated extract; C, RNase A–treated spindle assembly reaction treated with DMSO (control); I, RNase A reaction treated with ISGN (splicing inhibitor); T, RNase A reaction treated with triptolide (transcription initiation inhibitor); G, genomic DNA. Centromeric RNAs have a repeat length of 174 bp. Note that our primers are 106 bp apart and therefore amplify slightly smaller products. Centromere primers amplify many RNA species in extracts that have not been treated with RNase A (U). Essentially all of these species are degraded after RNase A treatment (R). Minor RNA species amplified under this condition may be double stranded or protected by other factors from degradation. The band in the control spindle assembly reaction (C) between 400 and 500 bp corresponds to a processed product. This product is missing upon splicing inhibition (I). This reaction (I) yields amplification products of tandem repeat–containing centromeric RNAs in a pattern very similar to that of amplified genomic DNA (G). These products are derived from monomer and dimer repeats contained in the tandem repeat–containing centromeric RNA that is produced in the absence of RNA processing. Monomer and dimer products are not amplified after processing, likely because of the removal of primer binding sites. (A) RT-PCR analysis of centromeric fcr1 ncRNA synthesized during mitosis in the presence of DMSO, ISGN, or TRIP. RT-PCR (left), no RT (reverse transcription) controls (center), and isolated RNA used for reverse transcription (right). (B) Second replicate experiment of A showing RT-PCR results (left) and isolated RNA used for reverse transcription (right). (C) Third replicate experiment of Fig. S2A showing RT-PCR results (left) and isolated RNA used for reverse transcription (right). (D) No RT controls for second and third replicates. (E) No RT controls for experiments shown in Fig. 2 B. (F) Assay from Fig. 2 B performed in the absence of interphase nuclei. No detectable centromere RNA synthesis occurs. (G) RT-PCR results (left) and no RT controls (right) of the gel in Fig. 2 D showing high molecular weight range of gel shown in Fig. 2 D. High molecular weight products in the supernatant lanes could be large centromeric RNAs that do not associate with CENP-C.

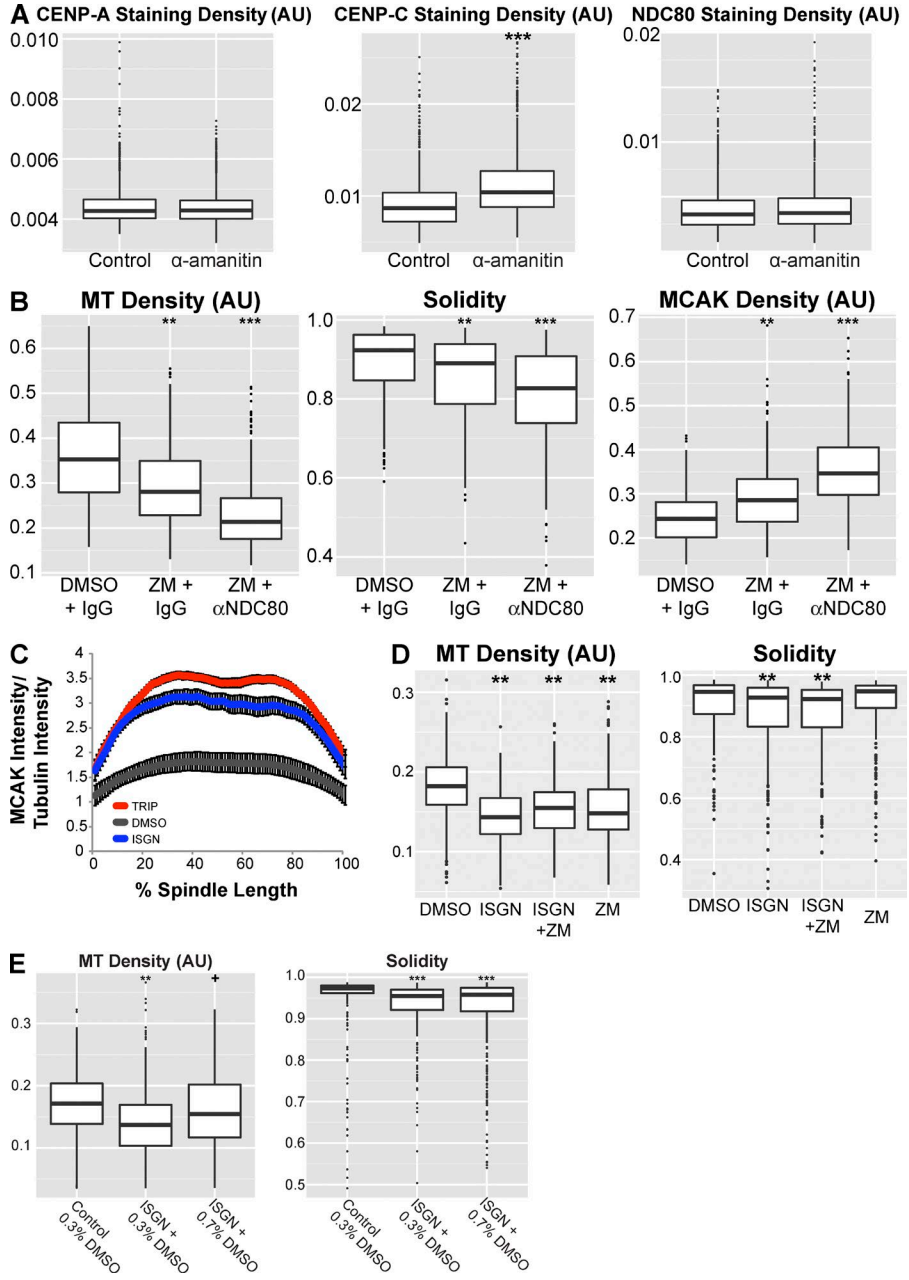

Figure S3. **α-Amanitin does not reduce CENP-A, CENP-C, and NDC80 localization; Aurora B and NDC80 inhibition together impair spindle integrity; and stabilization of spindle microtubules with DMSO does not fully rescue RNA biogenesis inhibition defects.** (A) Quantification of CENP-A (control, n = 1,113; α-amanitin, n = 2,493), CENP-C (control, n = 1,619; α-amanitin, n = 1,219), and NDC80 (control, n = 1,811; α-amanitin, n = 1,607) staining densities. Median CENP-C staining density increased 20.1% in α-amanitin–treated extract. (B) Quantification of spindle microtubule density, spindle solidity, and MCAK staining density in *X. laevis* extract treated with DMSO (n = 143) + nonspecific IgG, Aurora B inhibitor ZM447439 (5 µM) + nonspecific IgG (n = 273), or ZM447439 + αNDC80 antibodies (n = 329). Median microtubule density decreased 20.4% in ZM447439-treated extract and 39.8% in ZM447439 + αNDC80–treated extract. MCAK staining density increased 17.3% in ZM447439-treated extract and 42.1% in ZM447439 + αNDC80–treated extract. (C) Linescan quantification of MCAK staining in the dataset from Fig. 4 A. Plot shows mean intensity for spindles scanned along 100 length-normalized bins. Error bars show standard deviation. (D) Quantification of spindle microtubule density and spindle solidity in *X. laevis* extract treated with DMSO (n = 188), ISGN (n = 474), ISGN + ZM447439 (n = 227), or ZM447439 (n = 301). Median microtubule density decreased 21.3% in ISGN-treated extract, 14.9% in ISGN + ZM447439–treated extract, and 18.6% in ZM447439-treated extract. (E) Quantification of spindle microtubule density and spindle solidity in extracts treated with solvent control (0.3% DMSO, n = 198), ISGN (0.3% DMSO, n = 266), or ISGN + DMSO (0.7% DMSO, n = 322). Note that because DMSO is the solvent for ISGN, 0.3% is the minimum amount of DMSO that can be added to control reactions. Median microtubule density decreased 20.2% in ISGN + 0.3% DMSO–treated extract and 9.7% in or ISGN + 0.7% DMSO. In all cases, box plot mid-horizontal lines are median values, top and bottom lines are first and third quartiles, whiskers correspond to the 1.5 times interquartile range, and single points are outliers. *, $P < 10^{-5}$; **, $P < 10^{-10}$; ***, $P < 10^{-15}$. AU, arbitrary units; MT, microtubule.

Table S1. **Primer sequences used**

Primer	Sequence (5′–3′)
U4 forward	AGCTTTGCGCAGTGGCAGTATCA
U4 reverse	TCAAGTCATCACGGCGGGGT
5S forward	CCTACGGCCACACCACCCTG
5S reverse	CCGACCCTGCTTGGCTTCCG
18S forward	CGCACGGCCGGTACAGTGAA
18S reverse	GTCAGCGCTCGTCGGCATGT
U2 forward	TCGCTTCTCGGCCTTTTGGCT
U2 reverse	TGCGTGGAGTGGACAGAGCA
H3 forward	CCAGCCGGGAATCGCTCTAGGA
H3 reverse	ACTCTTCCTGGCGGCCTTGGT
Fcr1 forward	TGCAAGTGTTCCTGTTGCTT
Fcr1 reverse	TGGGAAAGTTGTCAGGGCTG
U2 knockdown	CAGATACTACACTTG
Nonspecific knockdown oligo	GCGGACGCTACAATACCTCCCT